Supporting Information

Bismuth Oxide/Graphene Oxide Nanocomposite Membrane Showing Super Proton Conductivity and Low Methanol Permeability

Bailing Liu[a], *Dongming Cheng*[a], *Haotian Zhu*[a], *Jing Du*[a], *Ke, Li*[a], *Hong-Ying Zang**[a,c], *Huaqiao Tan*[a], *Yonghui Wang*[a], *Wei Xing**[b], *Yangguang Li**[a]

1. **General Materials**
2. **Measurement**
3. **Ion exchange capacity, water uptake**
4. **Methanol permeability measurement**
5. **Impedance measurement**
6. **Figure S1.** (a) Structure unit of $\{H_6Bi_{12}O_{16}\}$; (b) 2D framework structure $\{H_6Bi_{12}O_{16}\}$; (c) 3D framework structure viewed along the c axis; (d) 3D framework structure packing viewed along the c axis.
7. **Figure S2.** (a) SEM image of $\{H_6Bi_{12}O_{16}\}$. Inset: Particle size distribution of$\{H_6Bi_{12}O_{16}\}$； (b) SEM image of $\{H_6Bi_{12}O_{16}\}$/GO. Inset: Particle size distribution of $\{H_6Bi_{12}O_{16}\}$/GO.
8. **Figure S3**. (a) High-resolution TEM images of $\{H_6Bi_{12}O_{16}\}$; (b) Amplified TEM images corresponding to the red frame regions in (a).
9. **Figure S4.** EDS elemental analysis of $\{H_6Bi_{12}O_{16}\}$/GO.
10. **Figure S5.** Powder X-ray diffraction of $\{H_6Bi_{12}O_{16}\}$/GO composite material at different condition to prove chemical and thermal.
11. **Figure S6.** FT-IR spectra of $\{H_6Bi_{12}O_{16}\}$/GO, $\{H_6Bi_{12}O_{16}\}$ and GO.
12. **Figure S7.** Raman spectra of $\{H_6Bi_{12}O_{16}\}$/GO, $\{H_6Bi_{12}O_{16}\}$, GO, respectively.
13. **Figure S8.** (a) XPS spectra of $\{H_6Bi_{12}O_{16}\}$/GO; (b) XPS spectra of Bi element.
14. **Figure S9.** The thermogravimetric analysis of $\{H_6Bi_{12}O_{16}\}$.
15. **Figure S10.** The thermogravimetric analysis of $\{H_6Bi_{12}O_{16}\}$/GO.
16. **Figure S11**. Nyquist plots for $\{H_6Bi_{12}O_{16}\}$ under different RH% at 303K.
17. **Figure S12.** Nyquist plots for $\{H_6Bi_{12}O_{16}\}$/GO composite membrane in aqueous solution at various temperatures
18. **Figure S13**.Typical response curves of the Nafion117 film sensor upon exposure to 43% RH and 97%RH at 1000 Hz.
19. **Figure S14.** Nyquist plots for $\{H_6Bi_{12}O_{16}\}$/GO under different RH% at 303K； Inset: the equivalent circuit models of the typical Nyquist plots fitted by the Zview Tools.
20. **Figure S15.** Nyquist plots for humidified $\{H_6Bi_{12}O_{16}\}$/GO (under 97% RH) from 0°C to -40 °C.
21. **Figure S16.** Negligible changes of proton conductivity of humidified $\{H_6Bi_{12}O_{16}\}$/GO during heating-cooling cycle at sub-zero conditions.

1. General Materials.

Bismuth nitrate (AR), and Graphite powder were purchased from Aladdin reagent (Shanghai) company, other chemicals (AR grade) were purchased from Sinopharm Chemical Reagent Company. Hydrogen peroxide (H_2O_2, 30 wt %) was obtained from Sinopharm Chemical Reagent Co. Ltd. The 0.1 M phosphate buffer solution (PBS pH 7.4), which was comprised of KH_2PO_4, Na_2HPO_4, was employed as a supporting electrolyte. All reagents in this research were used directly without further purification. Deionized water was used throughout the experiment. Graphene Oxide (GO) was prepared from natural graphite flakes applying a modified Hummer's method.

2. Measurement

Electrochemical measurements were performed using a three electrode configuration at room temperature. A glassy carbon electrode (GCE, 3 mm diameter) or a modified electrode served as a working electrode. A silver-silver chloride (Ag/AgCl, saturated KCl solution) and a Pt wire were used as reference electrode and counter electrode, respectively. In this study, all the sample solutions were purged with purified nitrogen (N_2) for 20 min to remove oxygen (O_2) prior to the beginning of a series of experiments and all experiments were carried out at ambient temperature. The cyclic voltammetry (CV) and amperometry were carried out by using a CHI660E workstation (CH Instruments, China). IR spectra were recorded on a Thermo Scientific Nicolet iS5 FT-IR spectrophotometer equipped with an iD5 diamond ATR attachment. Powder X-ray diffraction measurement was recorded radiation at room temperature on a Siemens D5005 diffractometer with Cu-Kα (λ = 1.5418 Å). RigakuMiniflex 600 diffractometer with Cu-Kα radiation (λ = 1.5418 Å) in a 2θ range from 5° to 70° with a 0.02° step at a scan speed of 5° min^{-1}. Brunauer−Emmett−Teller (BET) surface area, pore volume, pore size, and the adsorption−desorption isotherms were measured using a Micrometrics ASAP-2020 Mautomatic specific surface area and porous physical adsorption analyzer. The pore size distribution was measured by multiple Barrett−Joyner−Halenda (BJH) methods using adsorption branches of nitrogen adsorption−desorption isotherms. All the as-prepared samples were degassed in vacuum at 100 °C for 5 h prior to nitrogen adsorption measurements. Transmission electron microscopy (TEM) images were obtained by a JEOL 2100 transmission electron microscope operated at 200kV. Samples for TEM analysis were prepared by drying a drop of powder dispersion in absolute ethanol on carbon coated copper grids. Scanning electron microscopy (SEM) images were taken using a SU8000 ESEM FEG microscope operating at 5.0 kV.

The interrelated energy dispersive Xray detector (EDX) spectra were achievedby SU 8000 ESEM FEG microscope. To identify the carbon deposition, spent catalysts were measured by a Pyris Diamond thermogravimetric analyzer (TGA). The spent catalysts were heated from 50 to 800 °C at a heating rate of 10 °C/min at an air atmosphere with a gas flow rate of 50 mL/min.

3. Ion exchange capacity, water uptake

Ion exchange capacity (IEC) was measured in triplicate using a typical titration method. The weighed membrane was immersed into 25 mL of 0.05 M HCl solution and equilibrated for 48 h. After the immersion, HCl solution was back titrated by 0.05 M NaOH solution using phenolphthalein as indicator. IEC (mmol g^{-1}) value of membrane was calculated using the following equation:

$$IEC = (V_a - V_b) \times C_{NaOH} / W_d$$

Where W_d (g) is the dry weight of the sample, V_a is the volume of the blank sample, V_b is the volume consumed for the test sample, C_{NaOH} (mol/L) is the concentration of NaOH solution.

Water uptake (WU) of membranes are measured by the following steps: All the membranes were cut to 40 mm × 10 mm in size and immersed in deionized water for 48 h at 25 ℃ and 80 ℃. The water uptake W (%) was determined by the following equation:

$$W\,(\%) = [(W_w - W_d)/W_d] \times 100\%$$

Where W_w and W_d are the weights of the wet membrane and dried membrane, respectively.

4. Methanol permeability measurement

Methanol permeability of membranes was measured using liquid permeation equipment with two rooms. The membrane was cut into a round piece and sandwiched between two rooms which contained 8 M aqueous methanol solution and deionized water, respectively. The two rooms were continuously stirred during the test. The concentration of methanol in the deionized water was periodically determined by gas chromatography (GC). Methanol permeability was calculated using the following equation:

$$C_B\,(\mathrm{t}) = APC_A\,(t - t_0)/V_\mathrm{B}L$$

Where A (cm^2), L (cm) and V_B (cm^3) are the diffusion area, thickness of the membrane and the volume of permeated reservoirs, respectively. C_A and C_B (mol L^{-1}) are the methanol concentration in donor and receptor reservoirs, respectively. P (cm^2 s^{-1}) and $t - t_0$ are the methanol permeability and the time of methanol penetration, respectively.

5. Impedance measurement

Impedance measurement of the samples was performed on an IVIUM (Netherland) and Solartron electrochemical workstation. The sample was compressed to a pellet under a pressure of 15 MPa at room temperature. The pellet was attached to the surface of golden electrode. The proton conductivity was measured using AC impedance measurement. The relative humidity and temperature were controlled by using an HDHWHS-50 incubator. ZSimpView software was used to simulate impedance data to complete the Nyquist plot and obtain the resistance value. Proton conductivity of full hydration membranes (4 cm × 1 cm) was measured by the AC impedance method using Solartron electrochemical work station. The composite membrane was immersed in deionized water for 5 days before the impedance test until the acid protons on the surface were removed. The membranes were tested at different temperature using a modified four-probe AC impedance method over the frequency range 1Hz–1MHz. The proton conductivity is calculated as

$$\sigma = L/AR$$

Where σ is the ionic conductivity, R is the resistance, L is the thickness, and A is the area of the pellet. Activation energy linear fitting of the plot was obtained from the equation given below:

$$\sigma T = \sigma_0 \exp\left(- E_a / k_B T\right)$$

Where σ_0 is the pre-exponential factor, k_B is the Boltzmann constant, and T is the temperature.

6. Fuel cell performance

The preparation of $\{H_6Bi_{12}O_{16}\}$/GO/PVA membrane is described in detail as follows:

a) First, PVA (molecular weight ~145000) was dissolved in deionized water by stirring at 60 ℃ for 1 hour to make a 10 wt% solution. b) Desired amount of $\{H_6Bi_{12}O_{16}\}$/GO powder was dispersed in water (the concentration of $\{H_6Bi_{12}O_{16}\}$/GO was 3 mg mL^{-1}) under ultrasonic treatment for 2 hours. c) Subsequently, a specifically amount of $\{H_6Bi_{12}O_{16}\}$/GO solution with a concentration of 3 mg mL^{-1} was added into the above PVA (10wt%) solution and the mixture was stirred at 60 ℃ for 4 hours and then cooled to room temperature to obtain aqueous dispersion of $\{H_6Bi_{12}O_{16}\}$/GO/PVA mixture. d) 1.6 g (glutaraldehyde) GA (50 wt%) was added into the above $\{H_6Bi_{12}O_{16}\}$/GO/PVA mixture, followed by stirring for 2 min. The solution was cooled to room temperature, casted on a flat glass and dried at 60 ℃ for 12 hours. The $\{H_6Bi_{12}O_{16}\}$/GO/PVA membrane with the thickness of ~80 um was peeled off from the glass plate for the direct methanol fuel cell performance measurement.

Membrane Electrode Assembly and Single Cell Measurements: The DMFCs were fabricated by sandwiching $\{H_6Bi_{12}O_{16}\}$/GO/PVA membranes between two gas-diffusion electrodes. The catalyst ink used for the cathode was prepared by dispersing Pt nanoparticles (Johnson Matthey) into a 5 wt% Nafion aqueous solution. The catalyst ink used for the anode was prepared by dispersing Pt–Ru nanoparticles (Johnson Matthey) into a 5 wt% Nafion aqueous solution. Then cathode and anode catalyst inks were sprayed onto carbon papers (TGPH060, 20 wt% PTFE, Toray) to form cathode and anode, respectively. The catalyst loading and Nafion loading were 4 mg cm^{-2} and 60 wt% for both cathode and anode. The membrane electrode assemblies of $\{H_6Bi_{12}O_{16}\}$/GO/PVA membranes were prepared by mechanical extrusion for 30 s. The polarization curves of DMFCs were obtained by using a Fuel Cell Test system (Arbin Instrument Corp. USA) at 80 °C with an effective area of 3.3 × 3.3 cm^2. 1 M methanol solution was used as the reactant feed at the anode side with a flow rate of 5 mL min^{-1}, and humid oxygen was supplied to the cathode with a flow rate of 1 mL min^{-1}.

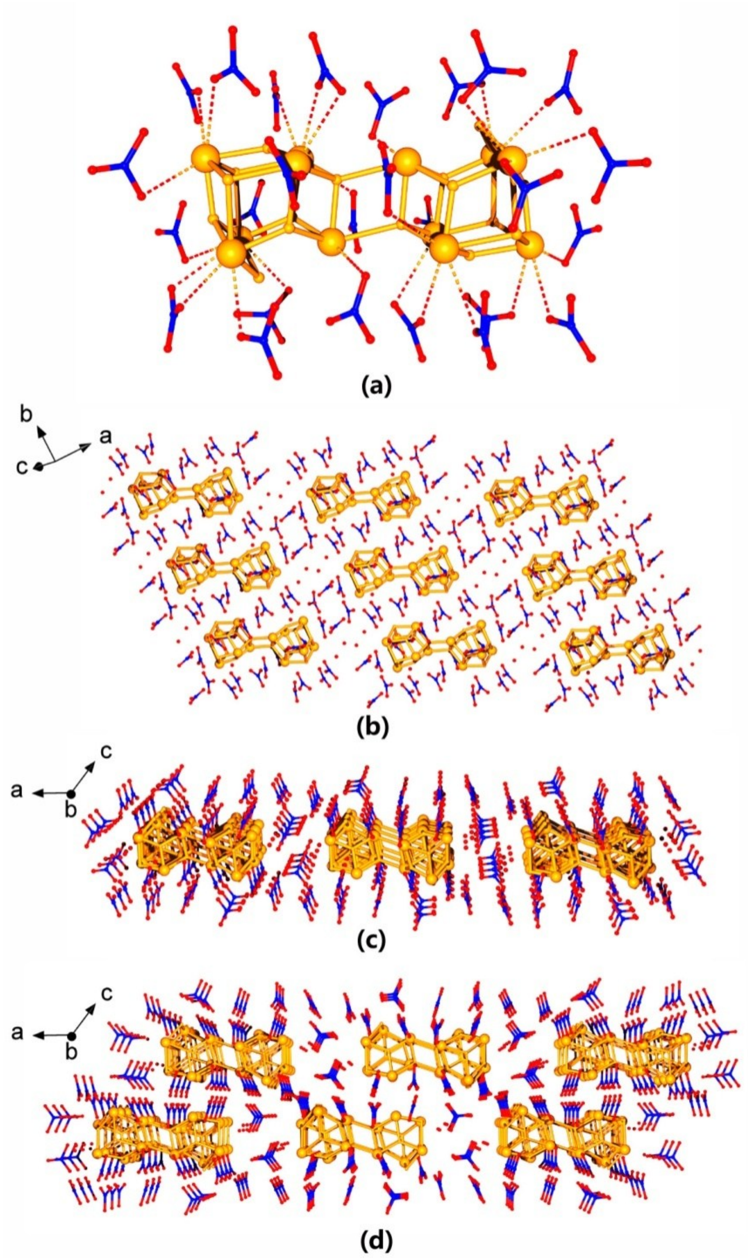

Figure S1. (a) Structure unit of $\{H_6Bi_{12}O_{16}\}$; (b) 2D framework structure $\{H_6Bi_{12}O_{16}\}$; (c) 3D framework structure viewed along the c axis; (d) 3D framework structure packing viewed along the c axis.

In the $\{H_3Bi_6O_8\}$ group the six Bi atoms are located at the corners of an octahedron with the O atoms above the centres of the octahedral faces. The three protonated oxygen atom (OH) groups and the bridging O atom with three Bi neighbours arranged pyramidally at longer distances, while the remaining four O atoms are linked to three more nearly coplanar Bi neighbours by shorter distances. A relatively strong hydrogen bond [2.78 (5) Å] can be observed between the O atom of the O…H group and the O atom of a water molecule. These free coordinated NO_3^- anions of the asymmetric unit act as counter anion, and the water molecule with O ascribed to NO_3^- anions is linked by four hydrogen bonds to four nearly tetrahedrally-arranged O atoms(Figure S1).These continuous hydrogen bond would benefit the proton conductivity.

In order to prevent the hydrolysis of bismuth nitrate, $Bi(NO_3)_3{\cdot}5H_2O$ was dissolved in HNO_3 (6 mol/L) with vigorous stirring at room temperature. Clarified bismuth nitrate solution was obtained. Then, a specifically amount of graphene oxide solution was added dropwise into the above solution, while adjusting the pH of the solution to 0 using 6 M NaOH. The 2D layered graphene oxide exists rich polar groups (such as hydroxyl groups, carboxyl groups and epoxide groups) to replace some of the nitrate anions of bismuth oxide clusters ($[H_6Bi_{12}O_{16}]$ $(NO_3)_{10}{\cdot}6(H_2O)$ $\{H_6Bi_{12}O_{16}\}$, and direct assembly of $\{H_6Bi_{12}O_{16}\}$/graphene oxide (GO) into membranes by electrostatic interaction and hydrogen bonding. The detailed synthesis process is as follows:

Synthesis of $\{H_6Bi_{12}O_{16}\}$/GO powder:

$Bi(NO_3)_3{\cdot}5H_2O$ (12.1 g, 0.025 mol) was homogenously dispersed in 10 mL nitric acid (6 mol/L) with vigorous stirring at room temperature. Then, 15 mL graphene oxide (10 mg/mL) solution was added dropwise into the above solution, while adjusting the pH of the solution to 0 using 6 M NaOH. Then, the solution was stirred for 12 h. The obtained brown precipitate was collected using centrifugation and washed with boiling water and acetone several times. Finally, the obtained product was dried at 80 °C in vacuum overnight with a yield of 60 %. The product was named as $\{H_6Bi_{12}O_{16}\}$/GO. For comparison, $[Bi_6O_5(OH)_3](NO_3)_5{\bullet}3H_2O$ (denoted as $\{H_6Bi_{12}O_{16}\}$) samples were prepared according to the previous literature (F. Lazarini, *Acta. Cryst.,* 1978, **B34**, 3169-3173).

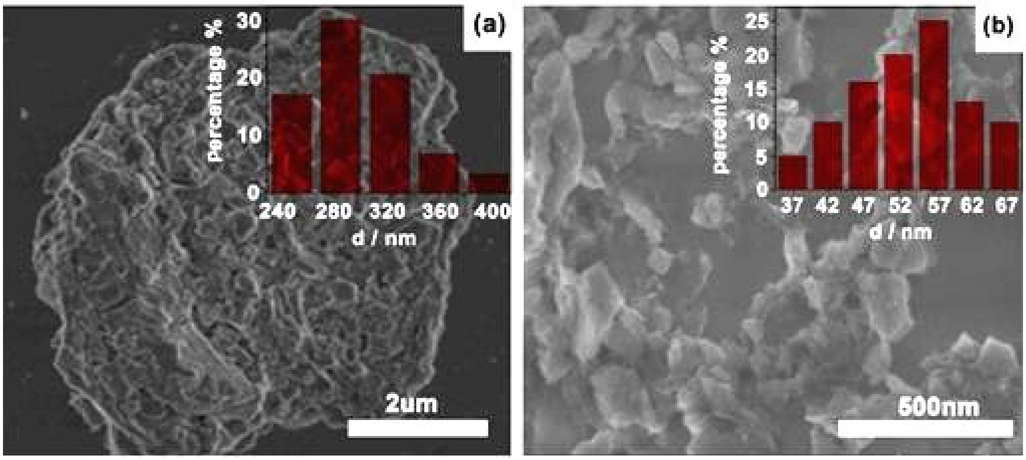

Figure S2 (a) SEM image of $\{H_6Bi_{12}O_{16}\}$. Inset: Particle size distribution of$\{H_6Bi_{12}O_{16}\}$; (b) SEM image of $\{H_6Bi_{12}O_{16}\}$/GO. Inset: Particle size distribution of $\{H_6Bi_{12}O_{16}\}$/GO.

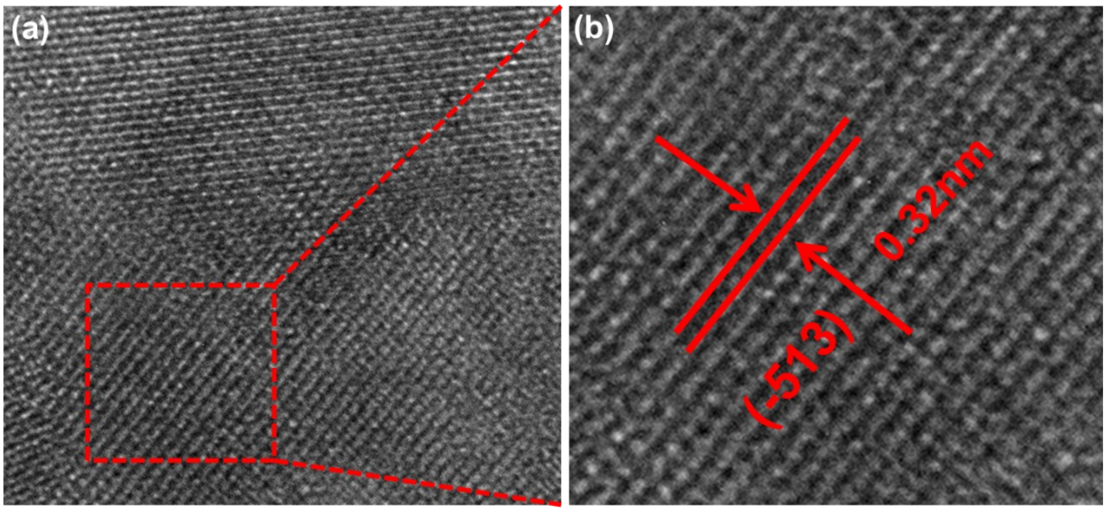

Figure S3 (a) High-resolution TEM images of $\{H_6Bi_{12}O_{16}\}$; (b) Amplified TEM images corresponding to the red frame regions in (a).

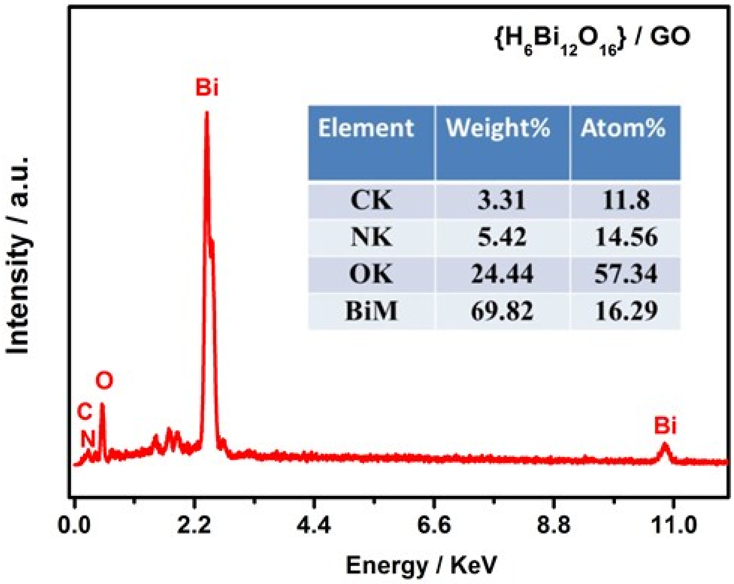

Element	Weight%	Atom%
CK	3.31	11.8
NK	5.42	14.56
OK	24.44	57.34
BiM	69.82	16.29

Figure S4 EDS elemental analysis of $\{H_6Bi_{12}O_{16}\}$/GO.

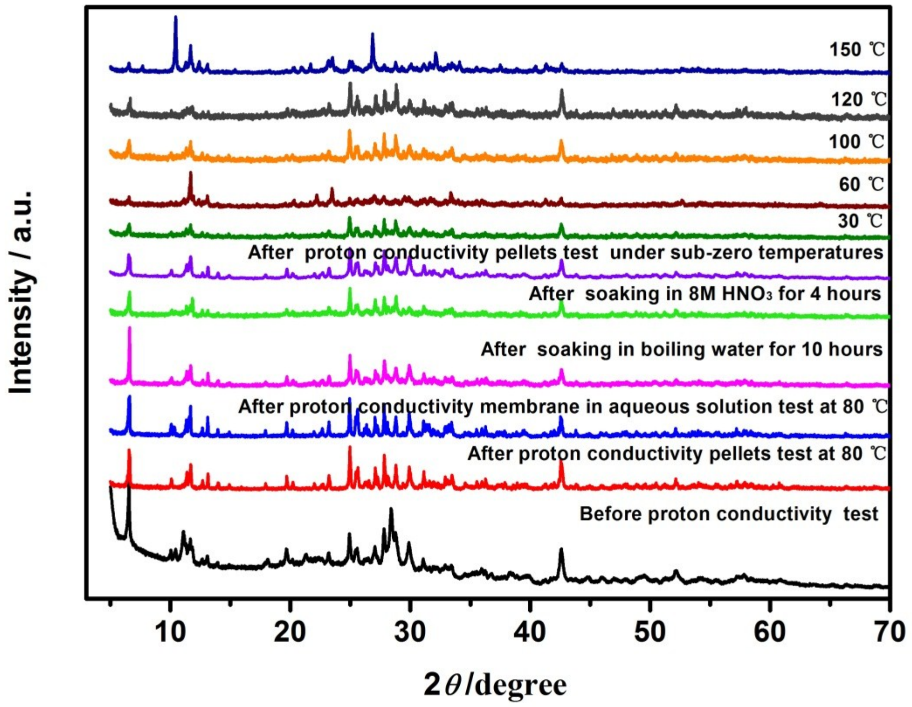

Figure S5 Powder X-ray diffraction of $\{H_6Bi_{12}O_{16}\}$/GO composite material at different condition to prove chemical and thermal stability.

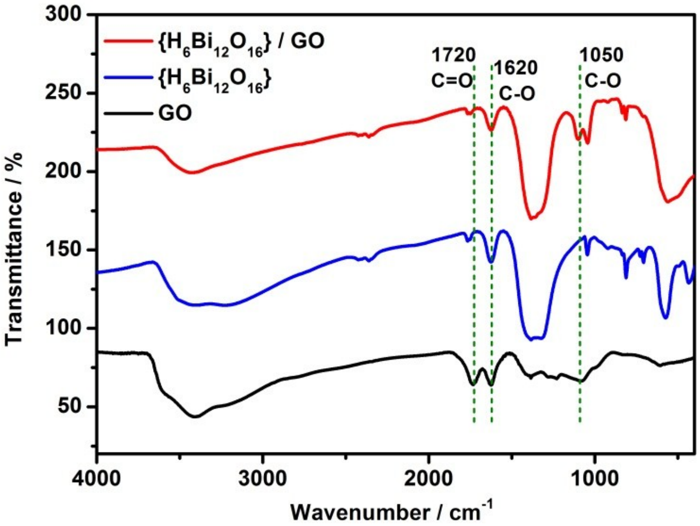

Figure S6 FT-IR spectra of $\{H_6Bi_{12}O_{16}\}$/GO, $\{H_6Bi_{12}O_{16}\}$ and GO.

The FT-IR spectra of GO, $\{H_6Bi_{12}O_{16}\}$ and $\{H_6Bi_{12}O_{16}\}$/GO were shown in Figure S6. The main absorption peaks of $\{H_6Bi_{12}O_{16}\}$ were located between 580 cm^{-1} and 1400 cm^{-1}, which can be attributed to stretching vibration and bending vibration of Bi–O and Bi–O-Bi. The representative absorption peaks of GO appeared at 3400 cm^{-1} (O–H stretching vibration), 1720 cm^{-1} (C=O stretching vibration of COOH groups), 1400 cm^{-1} (tertiary C–OH stretching vibration), and 1050 cm^{-1} (C–O stretching vibration) which were reported in the previous work. In the $\{H_6Bi_{12}O_{16}\}$/GO composite, intensity of peaks belonging to GO decreased or even disappeared in FT-IR spectrum, indicating strong hydrogen-bonding (O-H…O) formed between the oxygen-containing functional groups in GO and the surface oxygen atoms of bismuth oxide. The decreasing intensity of the absorption band of $\{H_6Bi_{12}O_{16}\}$/GO at 1700 cm^{-1} corresponding to skeletal vibration of graphene oxide sheets indicated that the graphene oxide was effectively combined with $\{H_6Bi_{12}O_{16}\}$ nanoparticles.

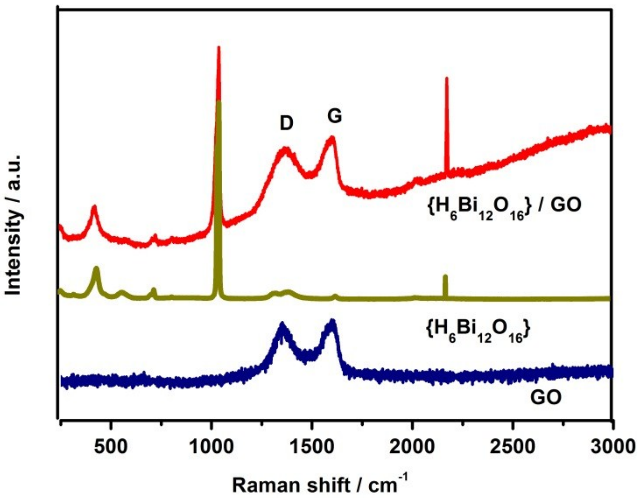

Figure S7 Raman spectra of $\{H_6Bi_{12}O_{16}\}$/GO, $\{H_6Bi_{12}O_{16}\}$, GO, respectively.

Raman spectra could further prove the existence of the graphene oxide sheets in the $\{H_6Bi_{12}O_{16}\}$/GO composite. As observed in Figure S7 the representative sharp peaks at 1080 cm^{-1} and 2100 cm^{-1} can be indexed to $\{H_6Bi_{12}O_{16}\}$ and the broad peaks at 1356 cm^{-1} and 1606 cm^{-1} are characteristic peaks for GO. The intensity ratio of the D (1356 cm^{-1}) and G (1606 cm^{-1}) band (D/G ratio) is 0.8665, implying the presence of graphene oxide. These results proved the combination of GO and $\{H_6Bi_{12}O_{16}\}$.

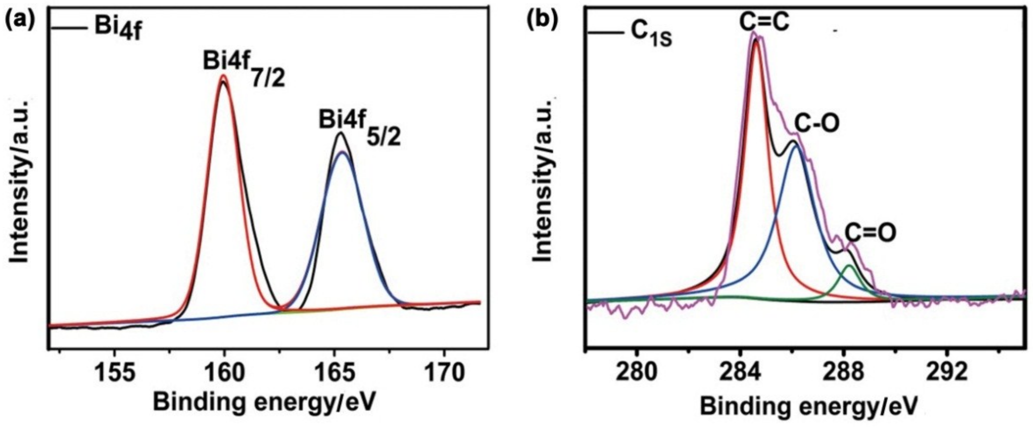

Figure S8 (a) XPS spectra of $\{H_6Bi_{12}O_{16}\}$/GO; (b) XPS spectra of Bi element.

High-resolution C_{1s} spectrum have a strong peak of C=C species (284.5 eV) and two relatively weak peaks of C-O (286.1 eV) and C=O (288.1 eV), which is in evidence of the introduction of graphene oxide. The high resolution XPS spectrum of Bi 4f exhibits two peaks at 159.9 eV and 165.3 eV assigning to Bi $4f_{7/2}$ and Bi $4f_{5/2}$, indicating the Bi^{3+} chemical state in the sample (Figure S8).

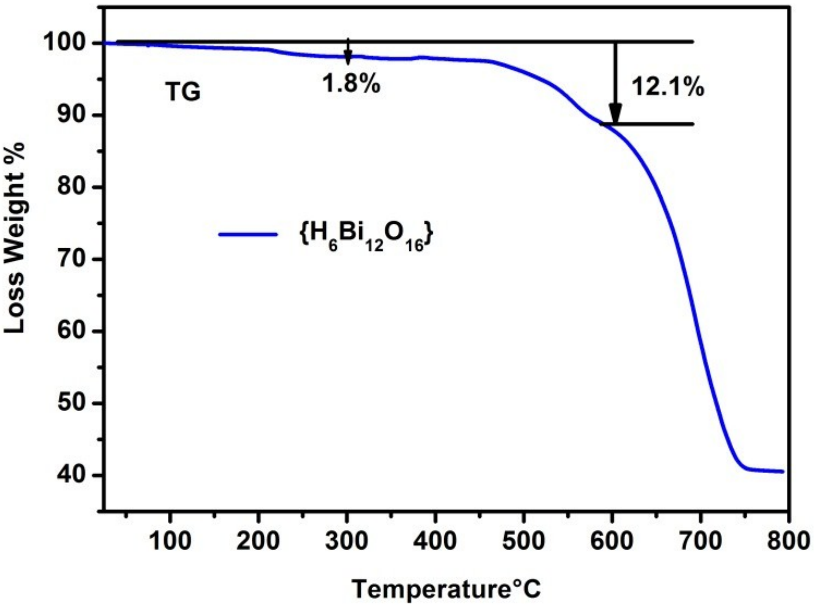

Figure S9 The thermogravimetric analysis of $\{H_6Bi_{12}O_{16}\}$.

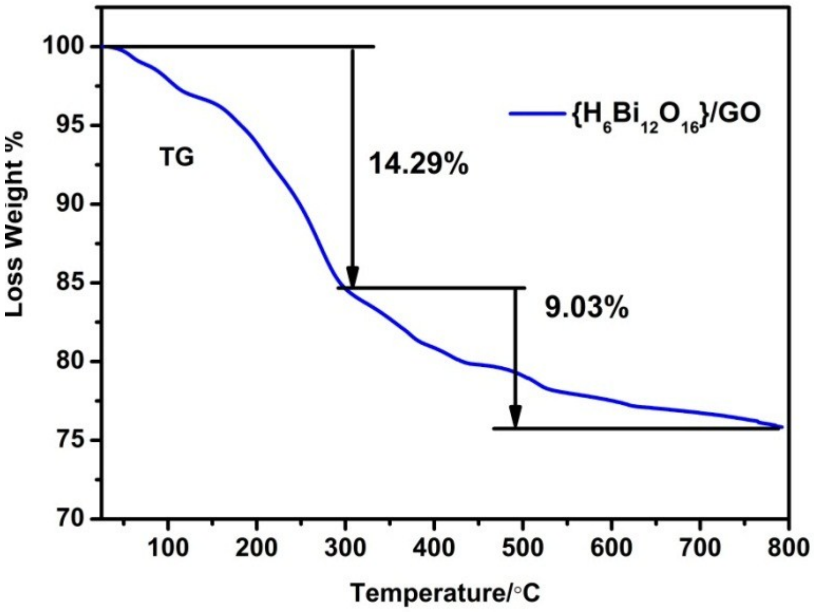

Figure S10 The thermogravimetric analysis of $\{H_6Bi_{12}O_{16}\}$/GO.

The thermal stability was investigated by thermogravimetric analysis (TGA) under nitrogen atmosphere. There were two steps of weight loss for $\{H_6Bi_{12}O_{16}\}$/GO as shown in Figure S10. The first weight loss from 30 to 300 °C was attributed to the removal of water molecules absorbed on the surface of $\{H_6Bi_{12}O_{16}\}$/GO and the loss of surface protonated oxygen atoms (-OH) and decomposition of nitric acid from bismuth oxide cluster. The total loss of water weight is about 14.3%. The 9.03% weight loss in the range of 300−800 °C corresponds to decomposition of the composite material skeleton. After that, the weight of the sample remains constant (Figure S9 and S10).

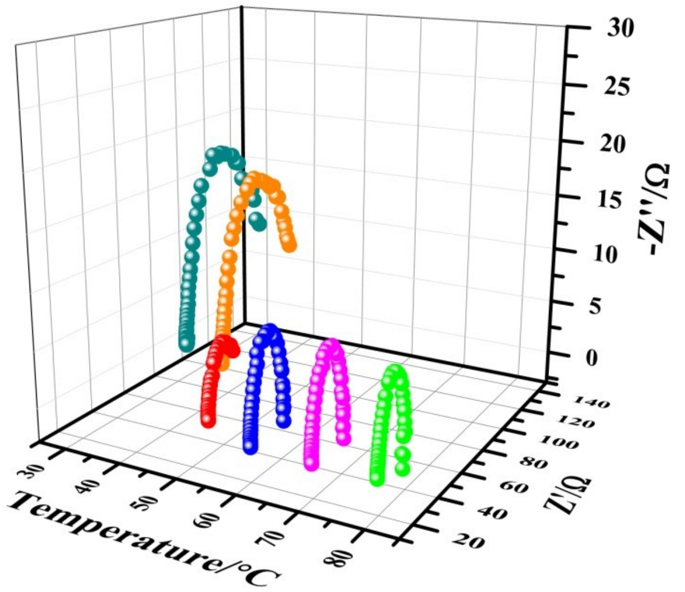

Figure S11 Nyquist plots for $\{H_6Bi_{12}O_{16}\}$/GO composite membrane in aqueous solution at various temperatures.

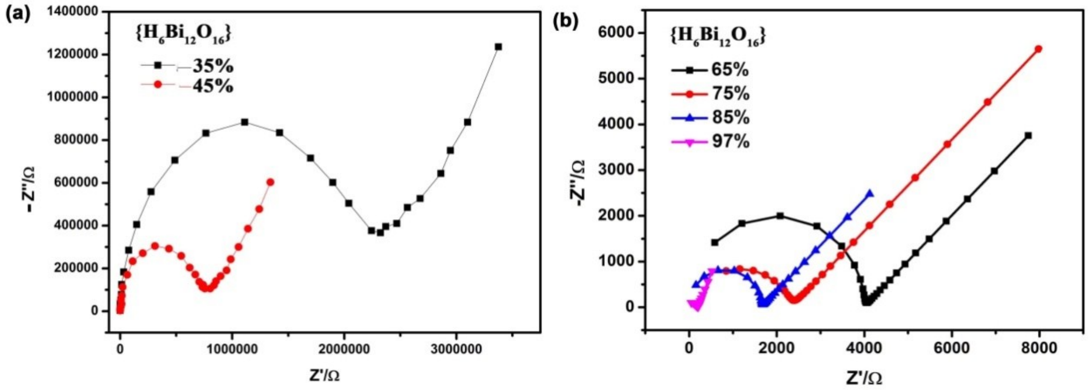

Figure S12 Nyquist plots for $\{H_6Bi_{12}O_{16}\}$ under different RH% at 303K.

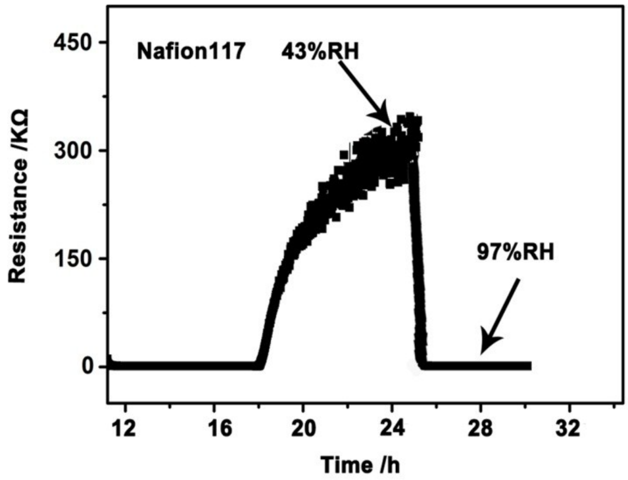

Figure S13 Typical response curves of the Nafion117 film upon exposure to 43% RH and 97% RH at 1000 Hz.

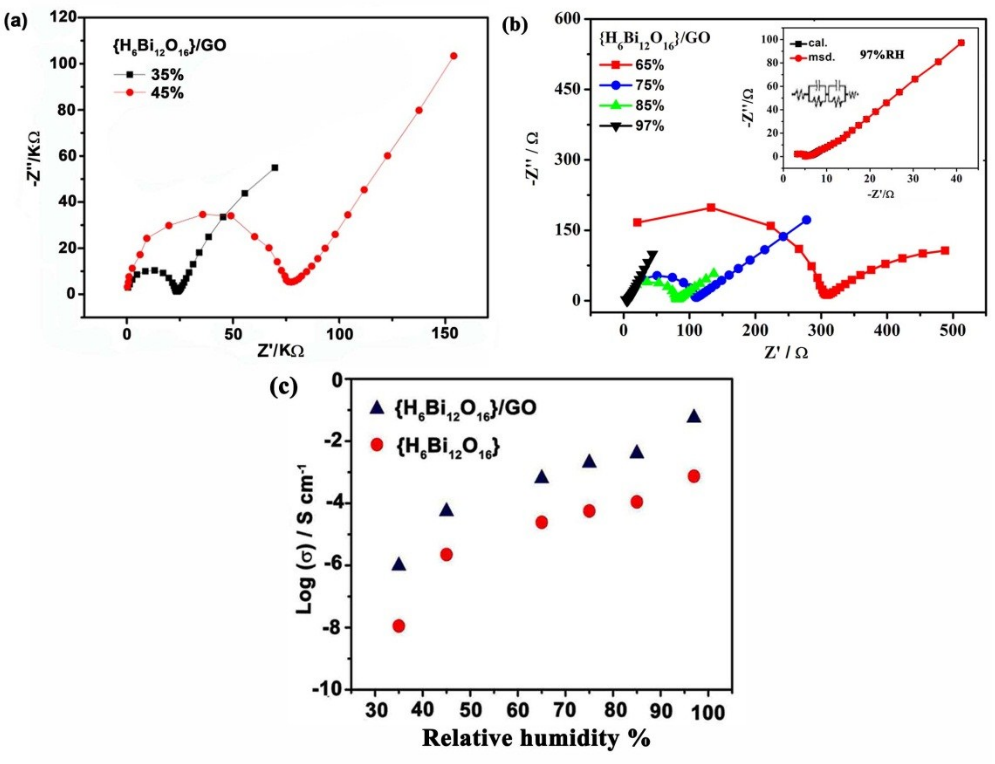

Figure S14 (a-b) Nyquist plots for $\{H_6Bi_{12}O_{16}\}$/GO under different RH% at 303K; Inset: the equivalent circuit models of the typical Nyquist plots fitted by the Zview Tools. (c) RH dependence of the conductivity (σ) for $\{H_6Bi_{12}O_{16}\}$ and $\{H_6Bi_{12}O_{16}\}$/GO at different relative humidity at 303 K.

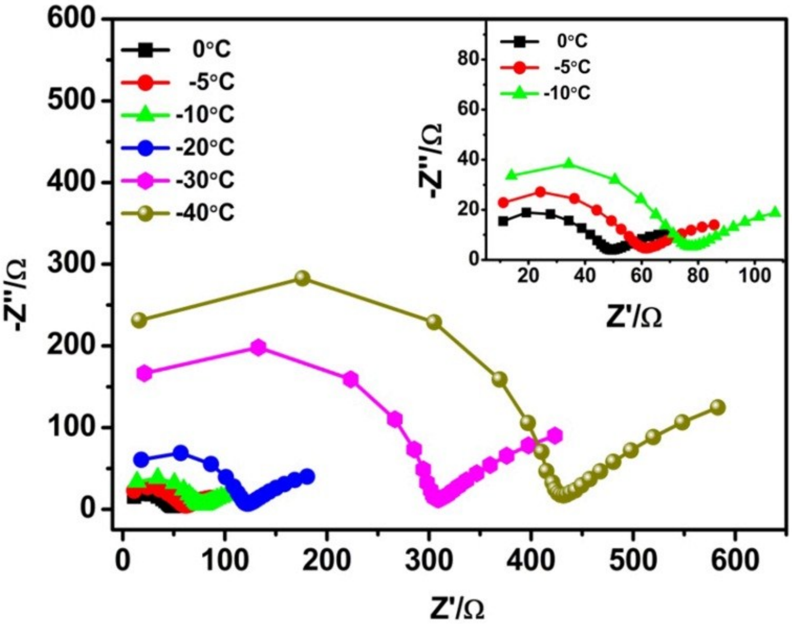

Figure S15 Nyquist plots for humidified {$H_6Bi_{12}O_{16}$}/GO (under 97% RH) from 0 °C to - 40 °C.

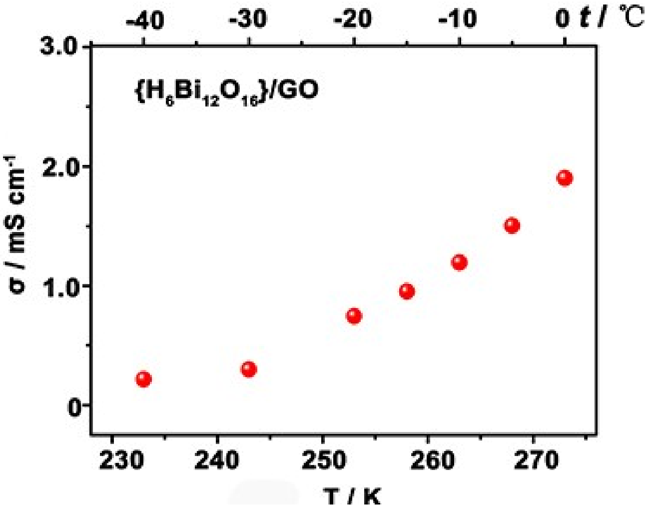

Figure S16 Proton conductivity for humidified {$H_6Bi_{12}O_{16}$}/GO from 0 °C to - 40 °C under anhydrous conditions.

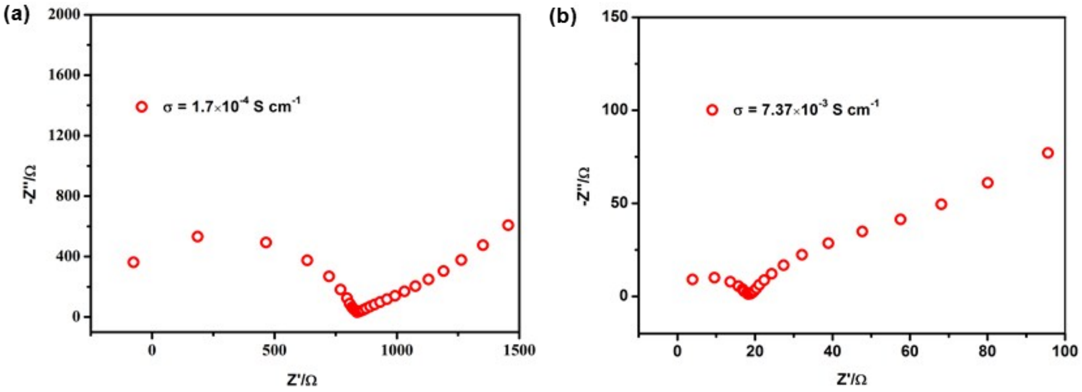

Figure S17 Nyquist plots for $\{H_6Bi_{12}O_{16}\}$/GO at different humidity (a) 75% relative humidity (D_2O); (b) 97% relative humidity (D_2O) at 303K.

The $\{H_6Bi_{12}O_{16}\}$/GO exhibited a proton conductivity of 1.7×10^{-4} S·cm^{-1} and 7.37×10^{-3} S·cm^{-1} at 75% RH (D_2O) and 97% RH (D_2O) and 30 °C, respectively (Figure S17). The conductivity values were lower than those of measured in H_2O (3.7×10^{-4} S·cm^{-1} and 5.5×10^{-2} S·cm^{-1} at 75% RH and 97% RH, respectively). The decreased proton conductivity in deuterate water was caused by the isotopic effect of deuterium. The isotopic effect supported our hypothesis that ionic conductivity was caused by proton transfer.

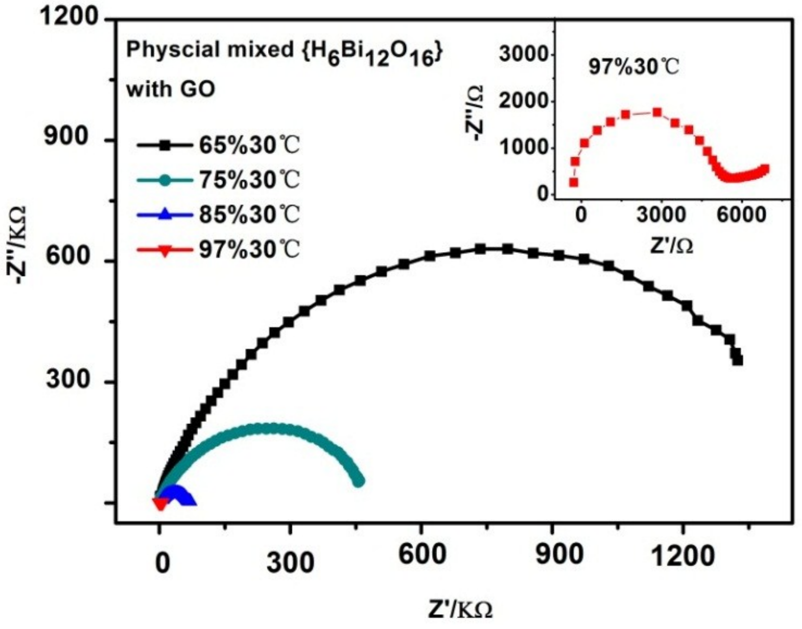

Figure S18 Nyquist plots for physically mixed $\{H_6Bi_{12}O_{16}\}\}$ with GO at different relative humidity at 30 ºC.

To investigate whether physical mixture of $\{H_6Bi_{12}O_{16}\}$ and GO can have the same effect on proton conductivity, we directly mixed the above ideal crystalline $\{H_6Bi_{12}O_{16}\}$ bulk material with graphene oxide powder with the approximate weight ratio of 8:1 and then measured its conductivity. The observed proton conductivity of this physically mixed material was only from 1.1×10^{-7} $S\cdot cm^{-1}$ to 2.7×10^{-5} $S\cdot cm^{-1}$ under RH from 65% to 97%RH at 30 °C (Figure S18), which was much lower than those of our synthesized $\{H_6Bi_{12}O_{16}\}$/GO composite. This result suggested that chemically synthesized proton conducting materials might construct continuous long-range hydrogen-bonding networks between bismuth oxide nanocluster and graphene oxide, thus performing better and steadier water–mediated proton conduction.

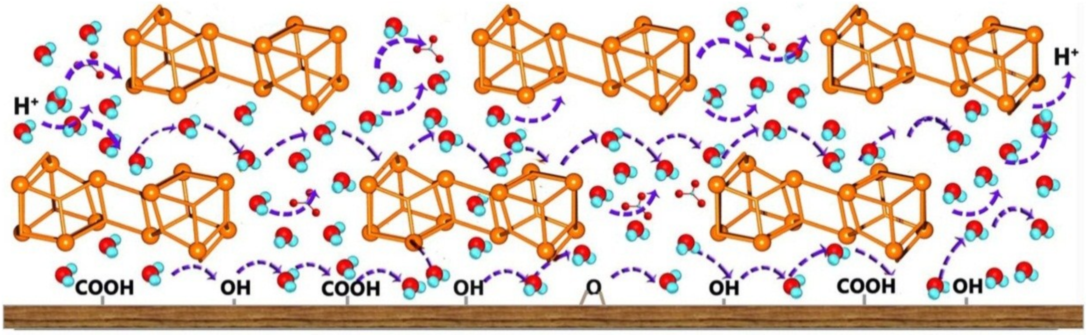

Figure S19 Proposed mechanism of proton conductivity for $\{H_6Bi_{12}O_{16}\}$/GO. Multiple proton conducting channels in the interlayer space are constructed by the abundant external oxygen atoms and the hydroxyl groups on the plane of substrate.

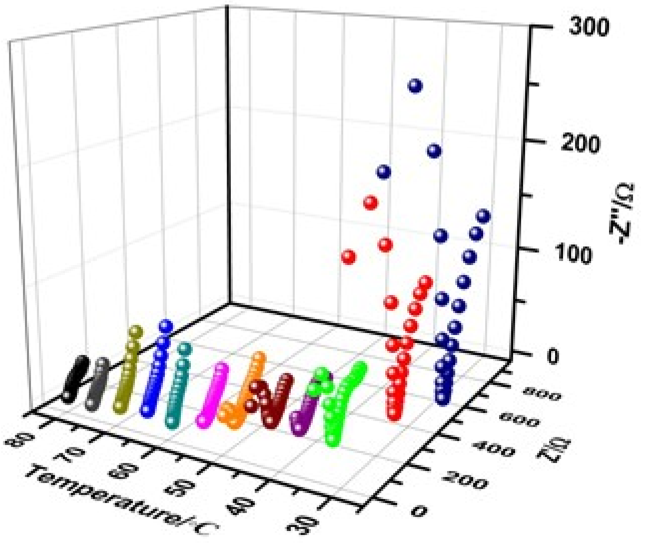

Figure S20 Nyquist plots for $\{H_6Bi_{12}O_{16}\}$/GO at 65%RH and various temperatures.

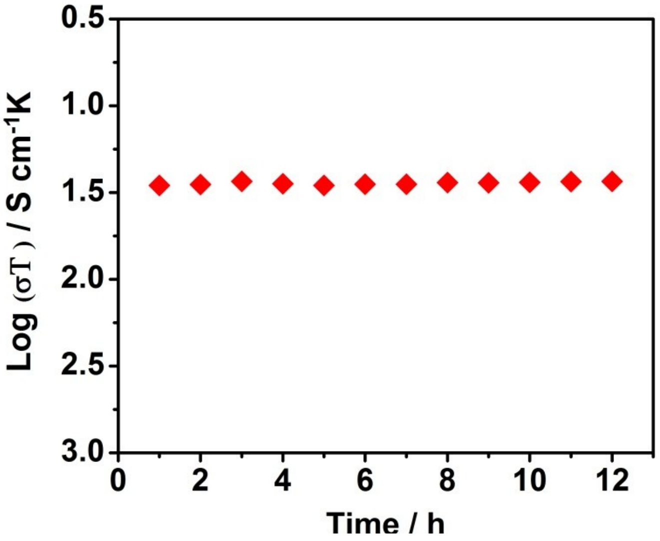

Figure S21 Long-term stability measurement at 80°C 97% for $\{H_6Bi_{12}O_{16}\}$/GO, the proton conductivity keeps 0.1 S·cm^{-1} for 12 h.

Table S1 Comparison of proton conductivity of {$H_6Bi_{12}O_{16}$}/GO, Graphene oxide, Nafion 117 and other materials.

References	Compound Name	Conductivity/ S cm^{-1}	E_a/eV	Conditions
1.	Nafion	~0.1	0.22	80 °C, 100%RH
2.	GO	~10^{-2}	----	100%RH
3.	DNA@ZIF-8 membranes	0.17	0.86	75 °C, 90%RH
4.	UiO-66(SO_3H)$_2$	8.4×10^{-2}	0.32	85 °C, 90%RH
5.	Prussian-blue NPs films	~1×10^{-1}	0.26	25 °C, 95%RH
6.	POMs-modified GO	1.02 × 10^{-2}	0.43	80 °C, 60%RH
7.	im@TPB-DMTP-COF	4.37 × 10^{-3}	0.38	150 °C
8.	(GO) / poly(phosphonic acid) core–shell nanosheets	0.035	---	51%RH
9.	SPEEK / S-UiO-66@GO	0.268	0.19	70 °C, 95%RH
10.	Nafion / UiO-66(SO_3H)$_2$	0.171	----	80 °C, 95%RH
This work.	**{$H_6Bi_{12}O_{16}$}/GO** **{$H_6Bi_{12}O_{16}$}/GO membrane**	**0.1(in vertical)** **0.564(in plane)**	**0.24**	**80 °C, 97%RH** **80 °C, in aqueous solution**

Table S2 IEC, WU, and Mechanical properties of different membranes.

Membrane	IEC (mmol g^{-1})	Water Uptake (%)	Young's modulus(MPa)	Tensile strength (MPa)
$\{H_6Bi_{12}O_{16}\}$/ GO	50.195	56.7	146.63	0.21
$\{H_6Bi_{12}O_{16}\}$pellets	7.695	13.6	----	----
Nafion 117	0.91	35	357	30.3

As shown in Table S2. The Ion exchange capacity of $\{H_6Bi_{12}O_{16}\}$/GO composite material displayed a relatively higher IEC of 50.195 mmol g^{-1}, which is in the same order of the other inorganic proton-conducting membranes, while the IEC of pure $\{H_6Bi_{12}O_{16}\}$ was 7.695 mmol g^{-1}. This is probably because carboxyl and hydroxyl groups on GO-based composite materials can provide more ion exchangeable groups. Water uptake was one crucial parameter for high-performance PEM fuel cells. The water uptake of pure $\{H_6Bi_{12}O_{16}\}$ was 13.6%, while the water uptake of $\{H_6Bi_{12}O_{16}\}$/GO was increased to 56.7%. We speculated that this was mainly due to $\{H_6Bi_{12}O_{16}\}$/GO containing a large number of free dangle hydrophilic groups (-OH, -COOH), which would make the matrix store more water by capillary action compared with pristine material. Interestingly, the hydrophilic carboxylic acid groups were responsible for improving water uptake and also facilitate the proton transfer by contributing more available sites for ionic transport. Table 2 shows the mechanical properties of the composite membranes-$\{H_6Bi_{12}O_{16}\}$/GO and Nafion membrane. All the membranes were tested at room temperature under dry conditions. However, Tensile strength of $\{H_6Bi_{12}O_{16}\}$/GO membrane is about 0.21MPa. The values show the mechanical stability is poor. Brittleness is the intrinsic characteristic of inorganic materials. It is probably due to the weak molecular bond interaction between the composite components.

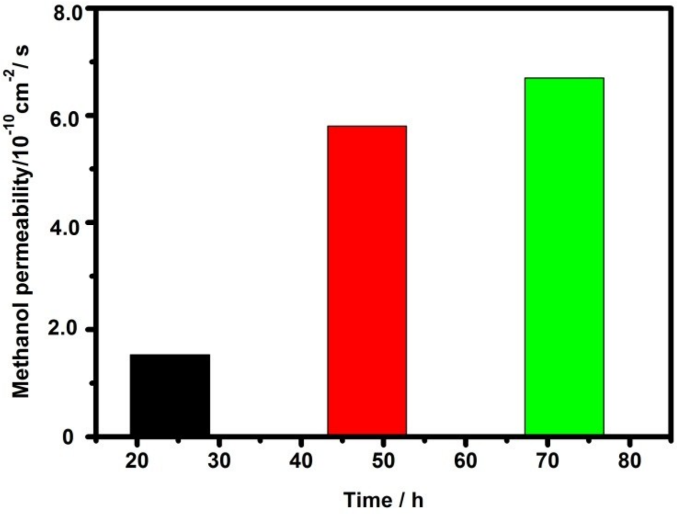

Figure S22 Methanol permeability of $\{H_6Bi_{12}O_{16}\}$/GO composite membrane at 298K.

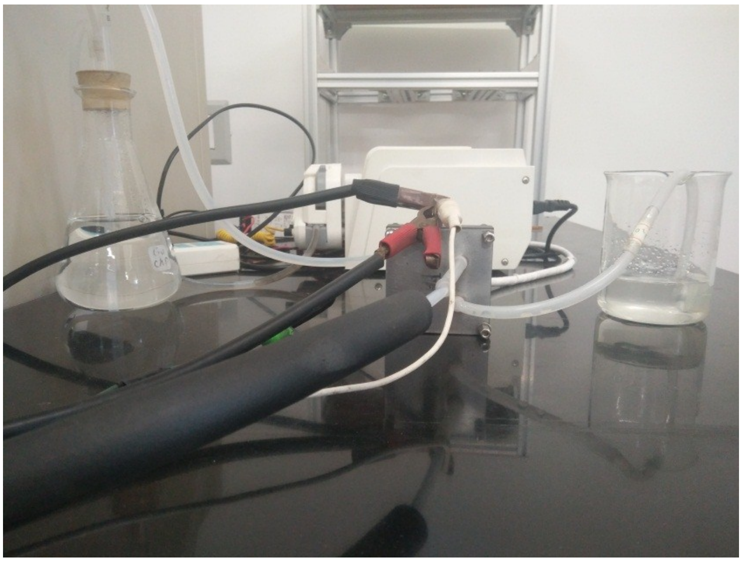

Figure S23. Membrane Electrode Assembly and Single Cell Measurements diagrams.

Table S3 Methanol permeability values of $\{H_6Bi_{12}O_{16}\}$/GO composite membrane at different time.

Membranes	Time / h	P_M (cm^2 s^{-1})
$\{H_6Bi_{12}O_{16}\}$/GO	24	1.53×10^{-10}
$\{H_6Bi_{12}O_{16}\}$/GO	48	5.81×10^{-10}
$\{H_6Bi_{12}O_{16}\}$/GO	72	6.61×10^{-10}

References:

1. X. Wu, X. Wang, G. He and J. Benziger, *J.* Polym. Sci., *Part B: Polym.Phys.,* 2011, **49**, 1437.

2. M. R. Karim, K. Hatakeyama, T. Matsui, H. Takehira, T. Taniguchi, M. Koinuma, Y. Matsumoto, T. Akutagawa, T. Nakamura, S. Noro, T. Yamada, H. Kitagawa and S. Hayami, *J. Am. Chem. Soc.,* 2013, **135**, 8097.

3. Y. Guo, Z. Q. Jiang, W. Ying, L. Q. Chen, Y. Z. Liu, X. B.Wang, Z. J. Jiang, B. L. Chen, X. S. Peng, *Adv. Mater.,* 2018, **30**, 1705155.

4. W. J. Phang, H. Jo, Lee, J. H. Song, K. Yoo, B. S. Kim and C. S. Hong, *Angew. Chem. Int. Ed.,* 2015, **54**, 5142.

5. K. Ono, M. Ishizaki, K. Kanaizuka, T. Togashi, T.Yamada, H. Kitagawa, M. Kurihara, *Angew. Chem. Int. Ed.,* 2017, **129**, 5531.

6. Y. W. Liu, S. M. Liu, X. Y. Lai, J. Miao, D. F. He, N. Li, F. Luo, Z. Shi and S. X. Liu, *Adv. Funct. Mater.,* 2015, **25**, 4480.

7. H. Xu, S. Tao and D. L. Jiang. *Nat. Mater.*, 2016, **15***,*722.

8. G. W. He, C. Y. Chang, M. Z. Xu, S. Hu, L. Q. Li, J. Zhao, Z. Li, Z. Y. Li, Y. H. Yin, M. Y. Gang, H. Wu, X. L. Yang, M. D. Guiver and Z. Y. Jiang, , *Adv. Funct. Mater.,* 2015**, 25**, 7502.

9. H. Z. Sun, B. B.Tang and P. Y. Wu, *ACS Appl. Mater. Interfaces,* 2017, **9**, 26077.

10. W. J. Phang, H. Jo, W. R. Lee, J. H. Song, K. Yoo, B. S. Kim and C. S. Hong, *Angew. Chem. Int. Ed .,* 2015, **54**, 5142.